3D EULER AND NAVIER-STOKES SIMULATION - A TOOL FOR DESIGN OPTIMIZATION OF TRANSPORT AIRCRAFT

Stefan Rill
Deutsche Aerospace Airbus, EF11
Bremen

Abstract

This paper reviews the usage of 3D Euler and Navier-Stokes simulation in the aerodynamic design process of civil transport aircraft at Deutsche Aerospace Airbus (DA). Considerable improvements in supercomputing and algorithm efficiency paved the way for Computational Fluid Dynamics (CFD) to become the second major discipline in aerodynamics beside experimental techniques.

The basic features of the DA code MELINA for 3D Euler and Navier-Stokes simulations will be described. In order to fully exploit the CFD potential, a hybrid design strategy has been developed that combines CFD, wind tunnel testing and simplified inverse design methods. To demonstrate the power of the strategy, we present two representative applications: The optimization of a high bypass ratio engine installation, based on 3D Euler simulations, and viscous transonic wing design, based on 3D Navier-Stokes.

Although CFD methods have matured such that they play a vital role in aerodynamic analysis and design, the simulation methods are yet not enough integrated in the overall aircraft design process. The same applies to simulation tools of other disciplines. In the final section, the author presents some new ideas to overcome these limitations.

Introduction

The success of a new generation civil transport aircraft on the world market strongly depends on the quality of its aerodynamic design with direct implications on the direct operation costs (DOCs) and on the ecology due to potential fuel burn savings. As a consequence, the aerodynamicists aim to improve the aerodynamic efficiency of civil transports even well below todays level. Optimistic estimations of the aerodynamic improvement potential for this kind of aircraft, range in the order of up to 30 percent compared to contemporary state-of-the-art technology. This improvement is expected to be realised by a tremendous reduction of the cruise drag by applying various new technologies like laminar wing design, improved engine integration etc.

A specific feature of the aerodynamic technolgies mentioned is, that they all involve complex 3D flow physics. In order to tackle these problems it is of essential importance to have, beside the wind tunnel facilities, additional tools available for aerodynamic design optimization. This gap has been filled by Computational Fluid Dynamics (CFD), that has matured to become the second major discipline in aerodynamic engineering in the last decade. This was possible due to dramatic improvements in supercomputing power as well as in algorithm efficiency. An impressive example for this evolution is the fact that today we are capable to solve a numerical problem in aerodynamics 5 million times faster than 20 years ago.

In Fig. 1 the historical development of methods for numerical flow simulation, as they are applied in aerospace industry, is depicted. We distinguish between the capability of the methods to treat increasing geometrical complexity of aircraft configurations and the power to capture complex flow physics. As expected, we observe a distinct trend

towards viscous compressible flow simulation for complete aircraft. The price we have to pay by increasing the complexity of the flow field is indicated in terms of the number of unknown variables in the resulting linear or nonlinear systems of equations.

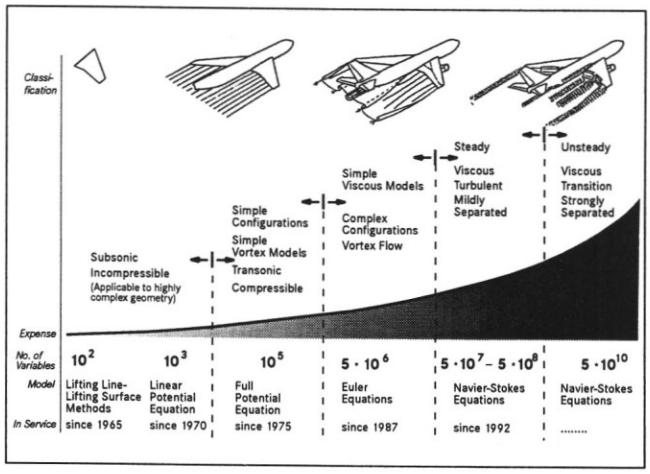

Figure 1: Numerical flow simulation - History.

Today, the methods have reached a level of sophistication that allows the simulation of the inviscid transonic flow field over a complete aircraft in cruise condition with tailplane and engines included. Within the scope of this paper, the author will present some new results of this type that have been obtained in the framework of daily aerodynamic design work at Deutsche Aerospace Airbus (DA). Nevertheless, the final goal is to simulate viscous flow around such a type of configuration or even a landing configuration with high lift devices applied. Since there is still a long way to go to reach such complexity, a very interesting intermediate step, from which important conclusions for the aerodynamic design can be drawn, is to simulate viscous flow around clean wing/body configurations. In the following sections we will present and discuss corresponding results and how they are used in the iterative aerodynamic design loop to improve on selected design parameters.

Later on we focus the attention to the integration of the CFD-methods in the overall industrial scenario, including pre- and postprocessing as well as monitoring of the computation. We have already mentioned above, that CFD-methods have reached a level of sophistication that they play a vital role in the design process of aircraft. The same applies to simulation methods in other disciplines like flight mechanics, structures, engine design etc. But there is still one major step left and that is to put the pieces together and integrate the individual simulation tools in one overall interdisciplinary software environment.

Another aspect of future working scenarios in aerospace industry is international cooperation. Although today most of the projects are carried out in international cooperation, we still lack an adequate environment to do that efficiently. But with the advent of international high speed networks this problem will be overcome. In the final section the author will describe a scenario in which efficient cooperation in the field of aircraft design can be achieved by using audio/video communication in combination with supercomputing on high speed networks.

The Numerical Method

Governing Flow Equations The Euler- and Navier-Stokes equations can be written in vector form

$$\frac{\partial}{\partial t}\int_V \vec{W}\, dV = -\oint_{\partial V} \bar{\bar{F}}(\vec{W})\cdot\vec{n}\, dO \qquad (1)$$

where $\bar{\bar{F}}$ is the flux tensor and $\vec{W} = (\rho, \rho u, \rho v, \rho w, \rho E)$ is the vector of conservative variables. ∂V is the surface of the control volume V and $\vec{n}$ is the outward unit normal vector on ∂V. The flux tensor $\bar{\bar{F}}$ may be divided into its inviscid and viscous part $\bar{\bar{F}} = \bar{\bar{F}}_i - \bar{\bar{F}}_v$. The inviscid flux tensor $\bar{\bar{F}}_i$ is given by $\bar{\bar{F}}_i =$

$$\begin{pmatrix} \rho u\vec{i_x} & \rho v\vec{i_y} & \rho w\vec{i_z} \\ (\rho u^2+p)\vec{i_x} & \rho uv\vec{i_y} & \rho uw\vec{i_z} \\ \rho uv\vec{i_x} & (\rho v^2+p)\vec{i_y} & \rho vw\vec{i_z} \\ \rho uw\vec{i_x} & \rho vw\vec{i_y} & (\rho w^2+p)\vec{i_z} \\ (\rho uE+up)\vec{i_x} & (\rho vE+vp)\vec{i_y} & (\rho wE+wp)\vec{i_z} \end{pmatrix}$$

whereas the viscous flux tensor $\bar{\bar{F}}_v$ is defined as

$$\bar{\bar{F}}_v = \begin{pmatrix} 0 & 0 & 0 \\ \sigma_{xx}\vec{i_x} & \sigma_{xy}\vec{i_y} & \sigma_{xz}\vec{i_z} \\ \sigma_{yx}\vec{i_x} & \sigma_{yy}\vec{i_y} & \sigma_{yz}\vec{i_z} \\ \sigma_{zx}\vec{i_x} & \sigma_{zy}\vec{i_y} & \sigma_{zz}\vec{i_z} \\ (\vec{v}\circ\vec{\sigma_x} - q_x)\vec{i_x} & (\vec{v}\circ\vec{\sigma_y} - q_y)\vec{i_y} & (\vec{v}\circ\vec{\sigma_z} - q_z)\vec{i_z} \end{pmatrix}$$

In the viscous flux tensor $\vec{\sigma_x}$ is defined as $\vec{\sigma_x} = [\sigma_{xx}, \sigma_{xy}, \sigma_{xz}]$. The pressure p can be calculated from

$$p = (\kappa - 1)\rho \left[E - \frac{\|\vec{v}\|^2}{2} \right].$$

where $\rho, \vec{v}, E$ and κ are the density, velocity vector, total energy per unit volume and ratio of specific heats of the fluid, respectively. The elements of the heat flux vector q and the stresses σ are given by the constitutive equations for a Newtonian Fluid. The viscosity μ is assumed to follow Sutherland's empirical power law. The heat conductivity is given by

$$k = \frac{\gamma}{\gamma - 1} \frac{\mu}{Pr}.$$

For turbulent flows, the eddy viscosity is determined using the Baldwin-Lomax or Johnson-King turbulence model. In the MELINA Euler- and Navier-Stokes code of DA, [1], the viscous flux tensor is simplified by the thin layer approximation.

Spatial Discretization A boundary-fitted finite volume mesh, generated by INGRID [2], is used for the spatial discretization of Eq. (1). In the cell vertex discretization the vertices of the finite volumes are taken as locations for the unknown variables $\vec{W}_{i,j,k}$

$$\frac{d}{dt}\vec{W}_{i,j,k} = \frac{-1}{V}_{i,j,k} \left[(\vec{Q}_i)_{i,j,k} + (\vec{Q}_v)_{i,j,k} \right] \qquad (2)$$

where $(\vec{Q}_i)_{i,j,k}$ and $(\vec{Q}_v)_{i,j,k}$ are the discrete inviscid and viscous flux balances, respectively. If we now add an artificial filter term to prevent odd-even decoupling or spurious high frequency oscillation modes we obtain

$$\frac{d}{dt}\vec{W}_{i,j,k} = \frac{-1}{V}_{i,j,k} \left[(\vec{Q}_i)_{i,j,k} + (\vec{Q}_v)_{i,j,k} - \vec{D}_{i,j,k} \right]. \qquad (3)$$

The artificial filter consists of blended 2^{nd} and 4^{th} differences of the solution vector that are scaled by the spectral radii of the Jacobian matrices associated with the ξ, η and ζ directions to account for large variations in the cell aspect ratios especially encountered in Navier-Stokes meshes. Various boundary conditions are implemented in MELINA to treat physically motivated boundaries like wall, farfield, etc. and algorithmic boundaries.

Solution Procedure For the time-stepping a hybrid, explicit 5-stage Runge-Kutta scheme is chosen. If we define the residual in Eq. (3) as

$$\vec{R}^k = Q_i(\vec{U}^k) + Q_v(\vec{U}^k) - \sum_{m=0}^{k} \gamma_{k,m} D(\vec{U}^m)$$

we obtain

$$\begin{aligned} \vec{U}^0 &= \vec{W}^n \\ \vec{U}^k &= \left(\vec{U}^0 - \frac{\alpha_k \Delta t}{V} \vec{R}^{k-1} \right), k = 1,2,3,4,5 \\ \vec{W}^{n+1} &= \vec{U}^5. \end{aligned} \qquad (4)$$

The coefficients $\gamma_{k,m}$ are chosen such that we obtain a hybrid (5,3) Runge-Kutta scheme that is to evaluate the filter terms only in every other Runge-Kutta step.

For convergence acceleration additional techniques like local time stepping, implicit residual averaging with variable coefficients, enthalpy damping (if applicable) and multi-grid acceleration are used. A special feature of the multi-grid procedure is that it does not distinguish between refined local sub-blocks and global mesh blocks such that the sub-blocks can be integrated in the multi-grid sequence and the convergence rate of the scheme is not degraded by using locally refined sub-blocks.

Aerodynamic Design Strategies

In order to exploit the aerodynamic improvement potential for civil transports of roughly 30 percent, the aerodynamicist rely, aside wind tunnel testing, on 3D numerical flow simulation. This is true since aerodynamic tasks like laminar wing design or engine integration etc. are inherently 3D problems which become nonlinear in the transonic regime, excluding traditional purely 2D approaches like airfoil design and optimization.

A typical task for the aerodynamic engineer is to design a wing geometry that features desired flow properties like minimal viscous drag and minimal wave drag at a prescribed Mach number and lift with acceptable off-design characteristics. Another problem might be, to find an optimal integration of the propulsion system to the airframe.

There are various possibilities to approach these tasks.

Obviously the most elegant method would be *direct optimization* of the geometry with respect to the desired specifications. Direct optimization means to vary the shape of the aerodynamic configuration (for example the wing) in a more or less sophisticated way and evaluate the resulting flow field around that configuration numerically with respect to the specifications [6]. Depending on the optimization strategy, that could mean up to 10000 evaluations. Unfortunately each evaluation of the flowfield in the transonic regime means one 3D CFD simulation, eather based on Euler- or Navier-Stokes equations. Instead of the dramatic developments in the field of CFD as well as in supercomputer power, these methods are still prohibitively expensive for complex configurations.

The second method to choose for the solution of the 3D design problem is the *inverse design* based on a prescribed pressure distribution. Inverse design methods are tailored to determine the aerodynamic geometry that yields a prescribed pressure distribution at a given Mach number. These methods are quite similar to the direct design methods in the sense that, if applied to 3D transonic problems, they are also based on geometry variation and evaluate the resulting flow field with respect to the prescribed pressure distribution, requiring as much flow simulations as the direct methods. A second problem is to define a desired pressure distribution. Especially this task requires lots of engineering know how and experience.

With this in mind, the engineers in the aerodynamic design department have developed a *hybrid design strategy* in close cooperation with the CFD group at DA. It can be seen as a sophisticated combination of numerical and experimental simulation tools with engineering know how and simplified design methods, Fig. 2. With this design strategy already various complex design problems have been tackled successfully, from which two will be presented here. The core of the design cycle is formed by the MELINA 3D flow simulation code based on the Euler- and Navier-Stokes equations and the flow evaluation and geometry modification step. The latter consists of various simplified design methods (like 2D nonlinear inverse design methods and 3D linear design methods) that have been developed in the aerodynamic design department and it is made of "engineering know how" that allows to push these simplified methods to the limits of their range of validity. Further details of this design strategy can be found in [3]. Among the numerous applications of the hybrid design strategy we pick two representative cases to demonstrate the power of the approach.

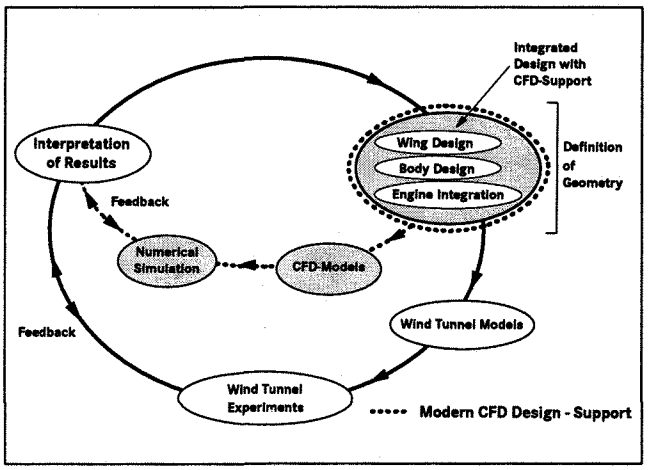

Figure 2: Hybrid aerodynamic design strategy.

Results

Euler Simulation for Complete Aircraft The installation of underwing high bypass ratio turbofans can lead to significant increase in installation drag due to the strong mutual interferences between the wing flow field and the flow around pylon and engine, such that the net reduction in specific fuel consumption (SFC) can be diminished considerably.

The hybrid design strategy was applied to the problem of improving such an engine installation on the MPC75 regional airliner project, [3]. The target was to sustain the clean wing isobar pattern even with pod and pylon mounted on the wing. As the design method in the geometry modification step, Fig. 2, a 2D nonlinear design method was used in combination with the concept of 2D analogous airfoil sections. These sections have been developed from the 3D pressure distribution, obtained with the MELINA code running in the Euler mode. To compensate the engine and pylon pressure pertubations on the wing, the geometrical differences of the analogous sections, determined with pod/pylon on and off, were superimposed on the original wing sections with inverted sign.

A first step in the campaign was to validate the MELINA Euler results with respect to wind tunnel experiments. Fig. 3 shows the result for a wing/body combination of the MPC75 with pod and pylon and flap-track-fairings (FTF) mounted under the wing. We see an astonishingly good correlation between experimental and numerical wing pressure distributions. Since the Euler equations allow only inviscid flow simulation, we applied the decambering technique, [4] to account for viscous effects in a simplified manner.

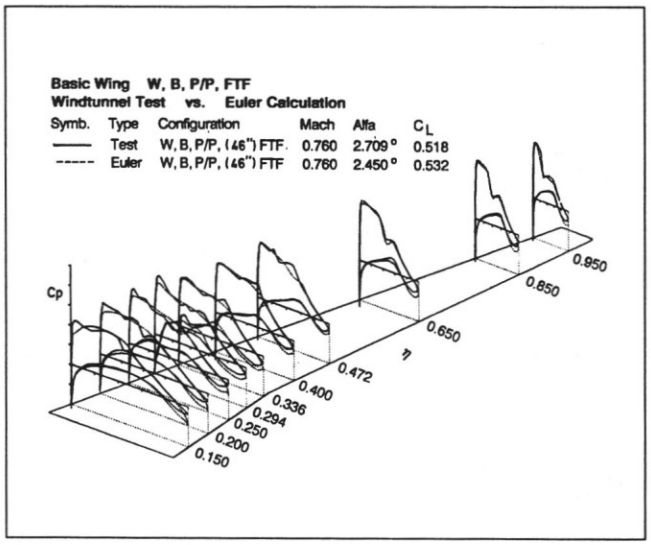

Figure 3: Comparison of test and Euler results - Wing/body/FTF.

In Fig. 4 the final result after several loops in the iterative hybrid design cycle is presented in terms of the local pressure distributions inboard and outboard of the pylon. "The comparison at the two span stations clearly indicates the successful application of the interference reduction concept. The suction peaks on the lower surface were nearly eliminated outboard of the pylon and only somewhat reduced inboard, which is due to geometrical constraints from the wind tunnel model layout. Outboard of the pylon the pressure distribution comes close to the clean wing distribution and on the upper surface the supersonic lift is restored", [3]. In the wind tunnel test it was found that this modification of wing lofting in the vicinity of the pylon lead to a net drag reduction of 1 percent, even with the geometrical restrictions due to the wind tunnel model.

For the type of aircraft configuration we have dealt with above, meshes with roughly 1 million

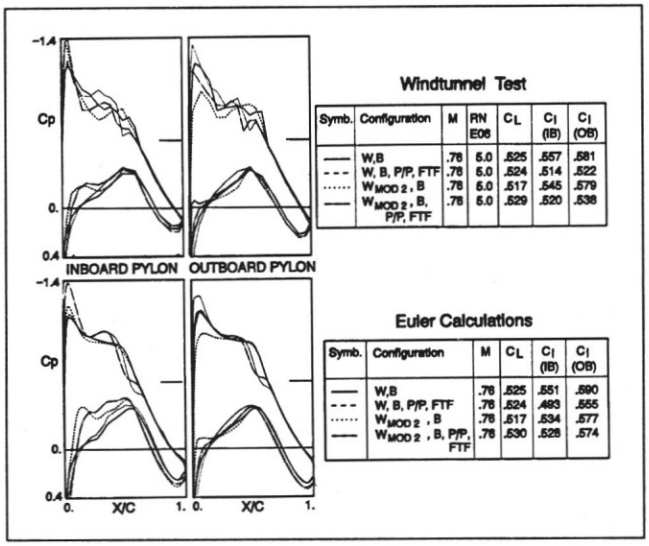

Figure 4: Comparison of section pressures.

grid points have been used to resolve the geometrical complexity. The CPU time required on a Fujitsu VP200 ranged from 1 hour for the clean wing case to 3 hours for the complete geometry if multi-grid acceleration was used. Only recently we have refined our capability to simulate inviscid transonic flow around complex configurations by applying MELINA to aircraft with four turbofan engines and four flap-track-fairings mounted on the wing. Fig. 5.

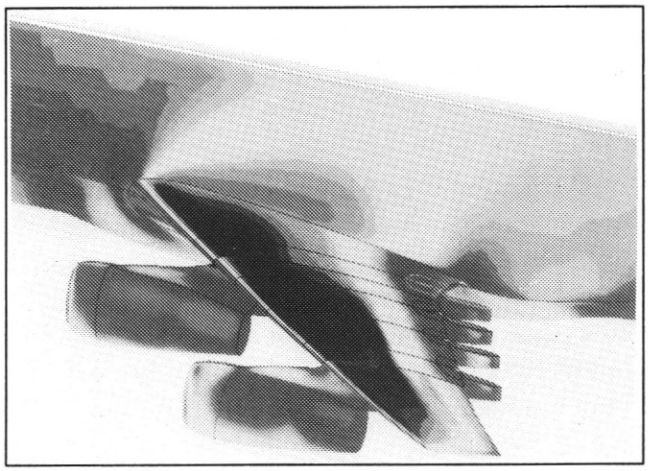

Figure 5: 4-engined configuration - Surface pressure.

Wing Design based on 3D Navier-Stokes Simulations Flow simulations on the basis of the Euler equations are limited to inviscid flow. Several methods have been developed in the past to

circumvent these limitation. The most popular one is to adopt the approach of Prandtl and to couple the inviscid "external" flow field, determined by the Euler equations, with the viscous flow that is confined to a boundary layer in the vicinity of the walls of the model. Another method is to add the boundary layer displacement thickness onto the geometry to account for the displacement effects of the boundary layer or even only to decamber the wing skeleton surface to simulate the decambering effects of the boundary layer.

Each of these methods has its limitations with respect to phyiscal generality or coding complexity. Especially the decambering technique, [4], which is based on the assumption of linearity of the flow field failes at high Mach numbers due to nonlinear effects. Hence at DA we decided to tackle viscous flow simulation directly by generalizing the MELINA code towards the solution of the Navier-Stokes equations. We described already above some aspects of the Navier-Stokes generalization but certainly we did not go into much detail since this is not the purpose of this paper.

As in the case of the Euler simulation it is mandatory to validate the computational Navier-Stokes simulation with repect to experimental results before they are to be used in the hybrid design strategy. This is especially true since the turbulence models used (the Baldwin- Lomax and Johnson-King models) are heuristic models and are only to be applied within their range of validity. Therefore a large validation effort has been undertaken in close cooperation with DLR in Braunschweig for Navier-Stokes simulations on the DLR-F4 wing/body configuration which reassembles a realistic transport aircraft configuration. The investigation revealed excellent results below the experimental buffet boundary, [5]. These results have been supported by validation campaigns at DA for various wing/body configurations of the Airbus family with similar successfull results.

The remaining part of this section is dedicated to a project were the design Mach number ΔMa_{Design} of a wing, with a design point already in the high transonic regime, was to be shifted by the increment of $\Delta Ma_{Design} = 0.03$ to a higher design Mach number without wing performance penalty. This was the first usage of the MELINA Navier-Stokes code in the hybrid design cycle.

Fig. 6 shows a comparison of the experimental and the Navier-Stokes wing pressure distribution of the reference wing/body combination at its (lower) design Mach number. For this computation we used $260*90*50 \approx 1.3$ million finite volumes in a C-O topology mesh with 30 volumes in the boundary layer. The correspondance of the data rectifies the application of the MELINA Navier-Stokes simuation for the kind of design optimization we have in mind within this study. There is only a small offset in shockposition in the outer wing part and a "strange" behaviour of the pressure distribution at the wing root section to be noted. A detailed 3D postprocessing revealed that the latter is due to a vortex that was formed at the wing/body junction at the upper wing side close to the trailing edge. Fig. 7 shows the corresponding streamlines and the surface pressure distribution in that region. The vortex was not found in the experiment and is obviously a consequence of the implementation of the thin layer approximation of the viscous terms which is not valid at the wing/body junction. Another source of error is that the eddy viscosities for the wing and body viscous layers were simply blended onto each other, depending on the distance of the field point from each of the walls.

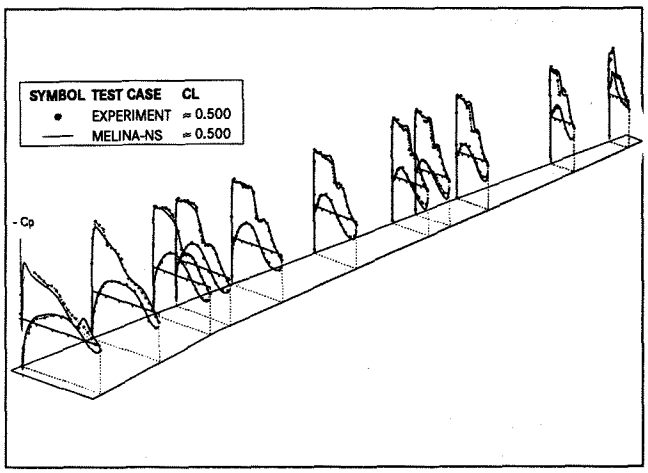

Figure 6: Reference configuration - Comparison of Navier-Stokes pressure distribution with experiment.

We adress the discrepancies in shockpositioning to the Baldwin-Lomax turbulence model that has been used in this particular simulation. This speculation is further confirmed by a subcritical computation for the same wing for which the agreement of experimental and Navier-Stokes data are found to be excellent, Fig. 8.

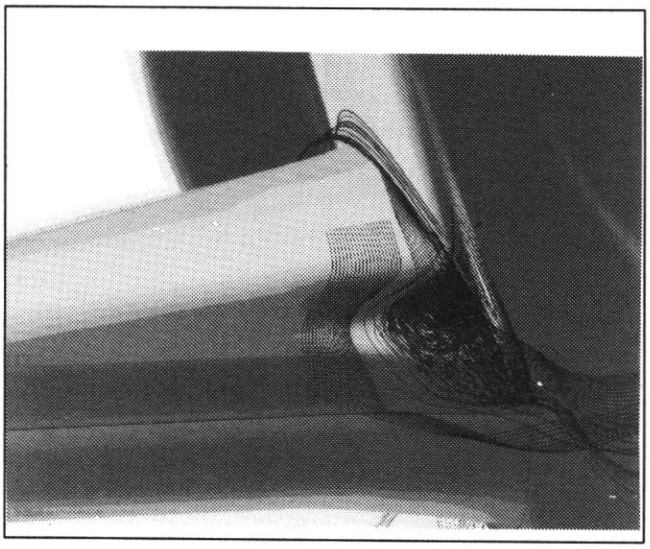

Figure 7: Vortex at wing/body junction - Streamlines.

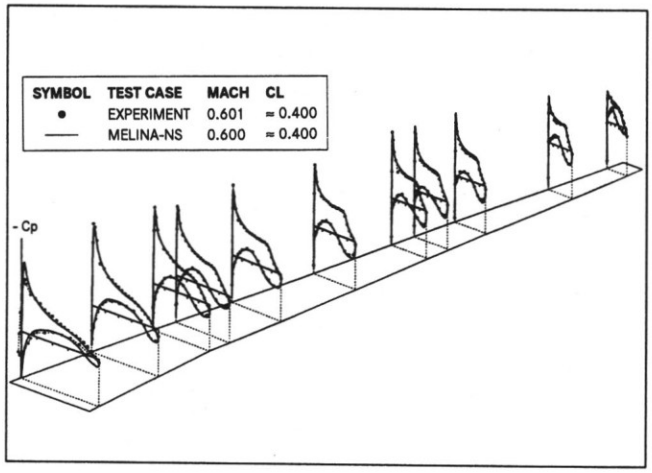

Figure 8: Reference configuration - Comparison of Navier-Stokes pressure distribution with experiment.

In Fig. 9 we present some more details of the transonic solution of the reference wing test case depicted in Fig. 6. We see the velocity profiles at three different points on the upper wing side expressed in terms of the streamwise and crossflow velocity components as well as the local velocity profile twist angle. In addition, the velocity profile $u_\tau = u/u^+$ is plotted against the dimensionless wall distance defined as $y^+ = \frac{yu^+}{\nu}$ with $u^+ = \sqrt{\tau_w/\rho_w}$ in order to resolve the viscous sublayer. In the latter plot, we also added the theoretical flat plate results for the viscous sublayer and the logarithmic law of the wall. The picture shows that:

- the boundary layer resolution is sufficient with approximately 30 cells in the boundary layer and a distance of the first grid line much less than 1 in terms of y^+
- the Navier-Stokes solution in the region of the viscous sublayer corresponds very well with the theoretical flat plate result.

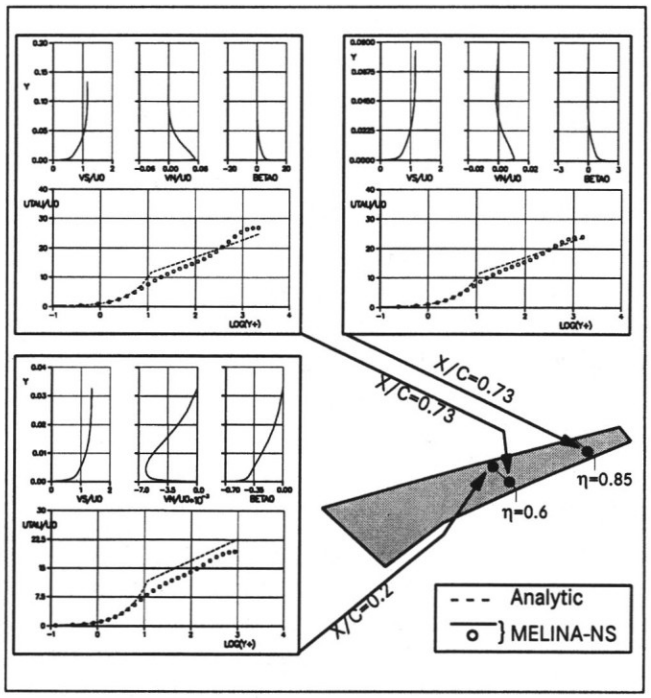

Figure 9: Resolution of the viscous layer - New wing design.

After this further validation of the Navier-Stokes method, the code was applied by the aerodynamic design department at DA to the aforementioned design problem in the hybrid design strategy. The resulting new design, that has been obtained after looping in the iterative design cycle, is shown in Fig. 10 in comparison with the upper wing Navier-Stokes pressure distribution of the reference wing. Note that the freestream Mach number of both cases differs by $\Delta Ma_{Design} = 0.03$.

The effect of the design modification can be esteemed if we compare the reference wing and the new design at the same Mach number. In Fig. 11 the upper wing side pressure distribution of both wings is shown at a freestream Mach number close to the higher Ma_{Design} of the new wing.

An important aspect of this new design was to shift the transonic drag rise of the wing to a higher Mach number. The evaluation of the new design

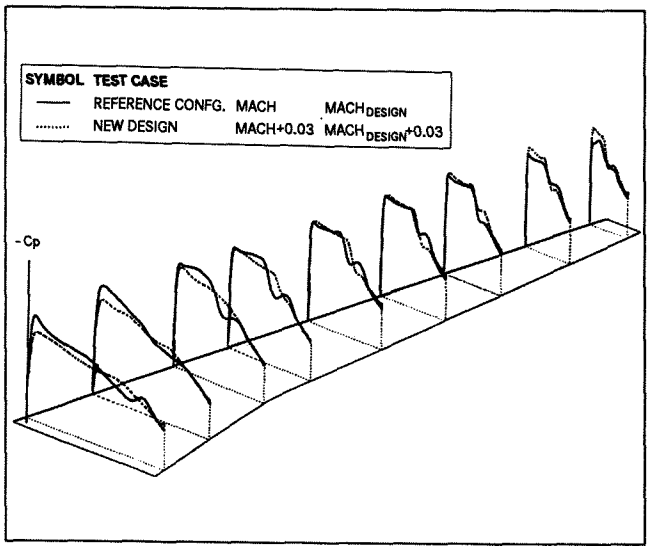

Figure 10: Comparison of reference wing and new design at their design Mach numbers.

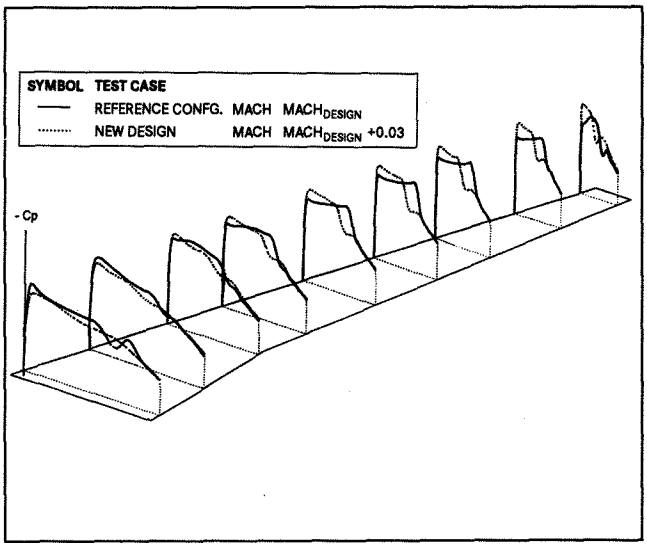

Figure 11: Comparison of reference wing and new design at the same Mach number.

with respect to this specifications requires the determination of the total drag of the viscous flow field around wing/body configurations simulated by the MELINA Navier-Stokes code. This is a non-trivial task. Although it is well known that the integration of the surface pressure distribution does not yield very reliable drag results, the pressure drag has been computed with that method in this study since a tool for drag integration on Trefftz planes is not yet fully operational at DA. Nevertheless the viscous drag may be very accurately determined from an integration of the skin friction distribution.

With this limitations in mind, Fig. 12 shows the transonic drag rise for the two configurations. First it is worthwhile to have a look at the experimental and numerical results for the reference configuration. We see that the total drag differs only by 10 dragcounts at the design Mach number of the reference wing and that the general trend in the transonic drag rise is predicted quite well with the Navier-Stokes method. This gives rise to the expectation that the predicted transonic drag rise of the new design wing is also quite reliable and that the design goal has been achieved and indeed, a last minute experimental result gave the proof of concept. In the wind tunnel test of the new design wing/body configuration a total drag value has been measured at the design point of that configuration, that differs only 5 dragcounts from the predicted Navier-Stokes results, see Fig. 12.

Future Working Scenarios

As we have already seen in Fig. 1 we have come a long way to reach the capability for viscous, transonic flow simulation around aircraft. But we have not yet reached our final goals. Further developments should aim in three different directions:

1. Increasing the speed and quality of numerical simulations: An impression of the aeronautical engineers targets can be drawn from Fig. 13 where the required computer speed for interdisciplinary unsteady problems like aeroelasticity is shown. In the same picture relief is indicated by the advent of massively parallel computers.

2. Improving on the integration of CFD-simulations and 3D-visualization into the product design process: This includes user-friendlyness of the simulation programs and especially the grid generation, which is one of todays major bottlenecks in CFD application. Although we find *concurrent engineering* in every modern management treatise, numerical flow simulation and simulation tools of other disciplines like structures, flight mechanics etc. are still is not enough integrated into the interdisciplinary engineering process of transport aircraft. This is especially due to the fact that there is no complete and unique definition of the aircraft available in the early

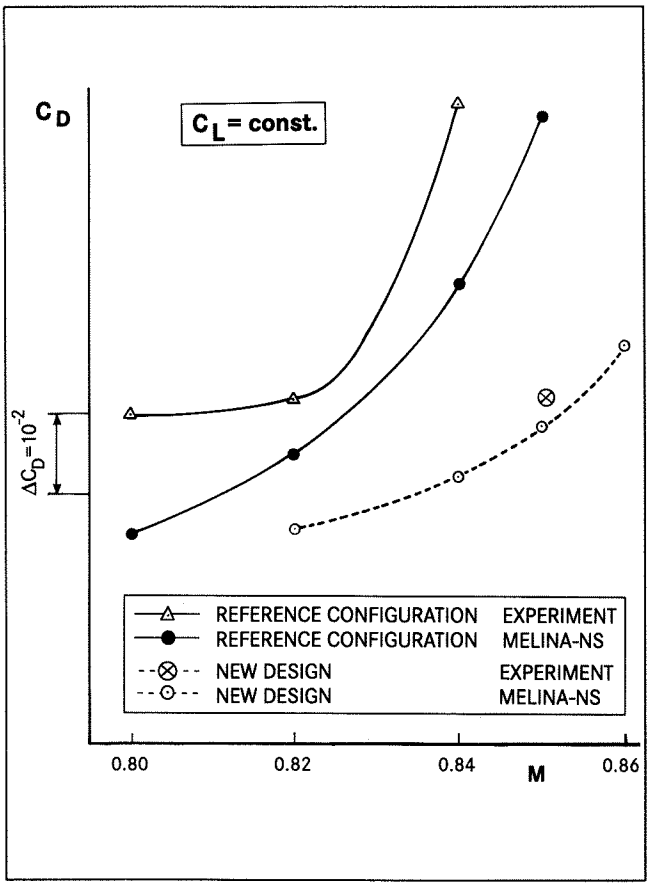

Figure 12: Transonic drag rise.

conception phase. An idea of how the concurrent engineering process could look like is depicted in Fig. 14.

3. Creating a platform for national and international cooperative work, based on supercomputing, visualization and multi-media communication on an international high speed network since most of the projects in aerospace industry are undertaken on an international cooperative basis. Within this context multiple European partners including DA, have applied at RACE, a European sponsoring agency, for a high speed network application project [8]. This PAGEIN project aimes to characterize the impact of key features of high performance computing on integrated broadband communication usage for aerospace industry. First results look very promising and can be viewed as a kernel for future working scenarios at DA, Fig. 15 and 16.

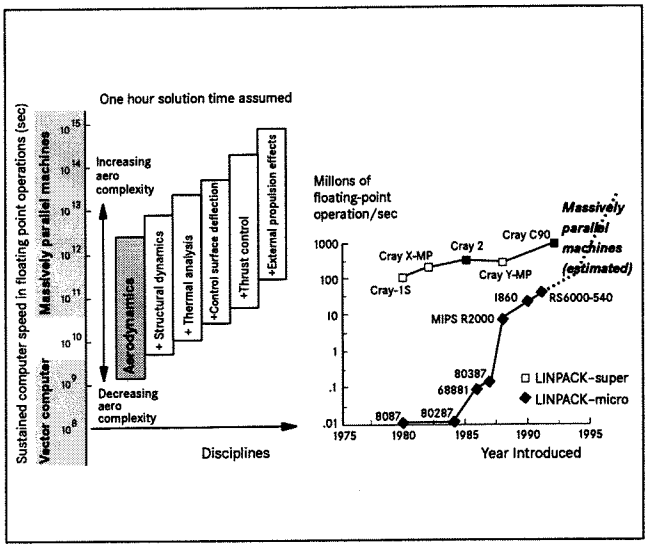

Figure 13: Computer speed estimates for multidisciplinary models, [7].

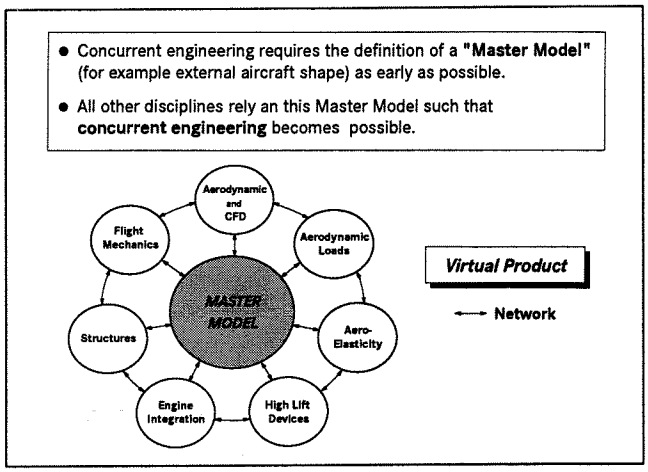

Figure 14: Interdisciplinary CAE - integration of simulation tools.

Conclusions

The purpose of this paper was to present a new aerodynamic design strategy based on 3D Euler- and Navier-Stokes simulations. The strategy was applied to an engine installation problem and to viscous transonic wing design with great success.

In order to fully exploit the potential of CFD and simulation methods in other disciplines it is essential to integrate the methods much better in the product design process. In the final section of the paper we have shown how the PAGEIN environment could serve as a kernel for an integrated design process that allows international interdisciplinary cooperative work.

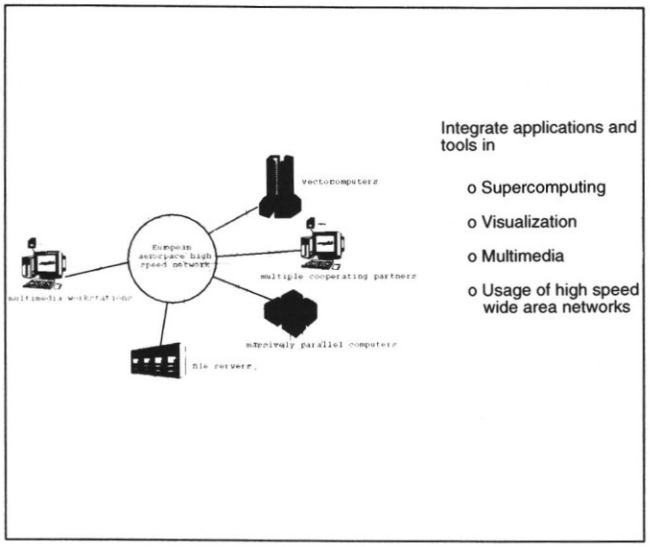

Figure 15: PAGEIN - Trans-european testbed.

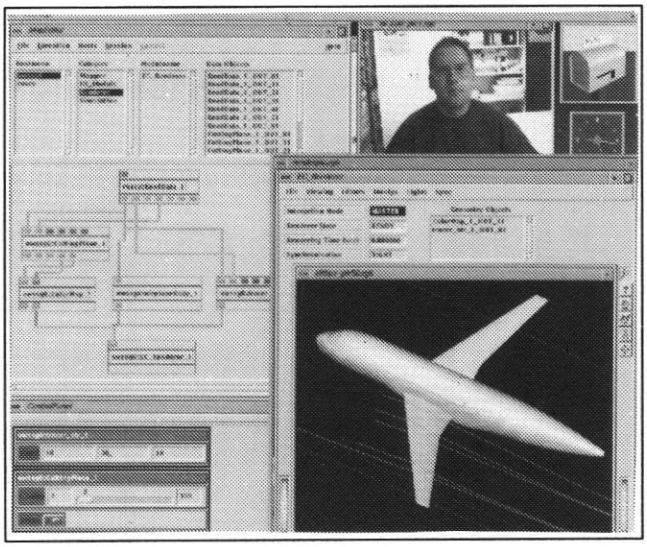

Figure 16: PAGEIN - Integration of simulation tools.

References

[1] Rill, S., Becker, K., "MELINA A - Multiblock, Multi-grid 3D Euler Code with Sub Block Technique for Local Mesh Refinement",ICAS Paper 92-4.3.R,*ICAS92*, Beijing, 1992.

[2] Becker. K., "Interactive Algebraic Mesh Generation for Twin Jet Transport Aircraft", it Proc. 3rd Int. Conf. Num. Grid Generation, Barcelona, June 1991.

[3] Greff, E., Becker, K., Karwin, M., Rill, S., "Integration of High By-pass Ratio Engines on Modern Transonic Wings for Regional Aircraft", *Aeronautical Journal*, January 1993.

[4] Rill, S., Becker, K., "Simulation of Transonic Inviscid Flow over a Twin-Jet Transport Aircraft",*Journal of Aircraft*, Vol. 29, Number 4, July - August 1992.

[5] Elsholz, E., Longo, J. M. A., "Navier-Stokes Simulation of a Transonic Wing-Body Configuration", Presented at European Forum: "Recent Developments and Applications in Aeronautical CFD" , Bristol, UK, Sept. 1-3, 1993.

[6] Van der Velden, A.J.M., "Aerodynamic Shape Optimization", AGARD R 803, April, 1994.

[7] Bailey, F.R., Dwoyer, D.L. and Nichols, L.D., "The New Challenge of Computational Aeroscience", ICAS Paper 92-4.1.1,*ICAS92*, Beijing, 1992.

[8] Grosso, R., Lang, U., Ryan, J. "CFD Experiment in a Distributed Simulation and Visualization System", *Proc. European Simulation Symposium ESS'93*, Delft, Holland, Oct. 1993.